Effects of iron precipitation and novel metal screw extrusion on electrical conductivity and properties of AA1370 aluminium

Geir Langelandsvik[a,d,*], Trond Furu[b], Oddvin Reiso[c], Hans Jørgen Roven[d]

[a] SINTEF Industry, 7034 Trondheim, Norway
[b] Norsk Hydro, Corporate R&D Headquarter, 0283 Oslo, Norway
[c] Norsk Hydro, R&D Centre, 6600 Sunndalsøra, Norway
[d] NTNU Norwegian University of Science and Engineering, Department of Materials Science and Engineering, 7034 Trondheim, Norway

ABSTRACT

In order to develop well-performing aluminium electrical conductors, the role of iron and processing method on electrical and mechanical properties was studied for an AA1370 alloy. Firstly, Ø3 mm cold drawn wires were subjected to a solid solution heat treatment (640 °C/1 h) followed by artificial aging at various temperatures in order to reveal the representative time-temperature-transformation (TTT)-diagram for Fe-rich precipitates. The highest precipitation rate occurred at 450 °C. Secondly, an identical AA1370 alloy was produced by the novel metal continuous screw extruder (MCSE) process into a new Ø3 mm wire. The as produced wire had a re-crystallised outer layer and an elongated fibrous structure having a typical ⟨0 0 1⟩ texture in the center region. TEM investigations revealed Fe-rich precipitates at grain boundaries thus impeding grain growth to some extent. The screw extruded wire processed at 450 °C had a high conductivity (64.2%IACS) while being softer (UTS ~65 MPa) than the cold drawn wire (UTS ~164 MPa, 61.9%IACS). The correspondence between strength and electrical conductivity for cold drawn and screw extruded wires was compared to literature data for pure and dilute alloys. The screw extruded wire outperformed other alloys as to electrical conductivity, while being among the materials having lowest strength.

1. Introduction

The use of aluminium as electrical conductors is gaining increased interest. With a conductivity-to-density ratio twice as high as copper, excellent corrosion properties, low cost and easy availability, aluminium is utilised for several electrical purposes [1–3]. Commercial pure aluminium alloys from the AA1XXX-series are commonly utilised as bus bars and high-voltage transmission wires. The aluminium alloys AA1350/AA1370 are especially important for electrical rod products, accounting for 80% of the total aluminium rod market [4].

The commercial AA1370 alloy possesses a reasonable combination of ultimate tensile strength (~85 MPa) and electrical conductivity (61.6%IACS) [5]. The material can be hardened by mechanisms such as solid solution strengthening, coherent precipitation, work hardening and grain refinement, in which all create discontinuities in the crystal lattice. As derived by Drude [6] and equated by Matthiessen [7], lattice defects scatter electrons and decrease the electrical conductivity. Thus, the strength-conductivity relation is often regarded as a trade-off [8].

Several authors point out solute lattice displacements as the major mechanism for decreasing the electrical conductivity [9,10]. Transition metals like Ti, V and Cr yield especially large lattice strains in aluminium. Hence, severe electron scattering reverting electrical properties has been experienced. This has commonly been overcome by additions of boron to the aluminium melt, creating metal borides with virtually no solubility in liquid aluminium. By letting precipitated borides sink to the furnace bottom, unwanted solutes are depleted without affecting the strength [2]. Incorporation of incoherent ceramic nanoadditives to increase the strength without redundant conductivity losses has also been demonstrated for electrical conductors [11,12].

The effect of foreign atoms, in or out of solid solution, on electrical conductivity in aluminium is given in Table 1 [13]. Iron, a common impurity element in commercial aluminium, influences electrical conductivity significantly. As seen from Table 1, iron in solid solution is 23 times more harmful to the electrical conductivity compared to precipitated iron aluminides. Obviously, driving iron out of solid solution is beneficial for electrical properties without losing strength. Although a maximum of 0.052 wt% iron can be dissolved by the aluminium matrix [14,15], even small amounts in solid solution implies a remarkable

Table 1
Effect of alloying elements on electrical conductivity in aluminium [13].

Element	Decrease in conductivity [%IACS/wt%]	
	In solution	Out of solution
Cr	39.03	4.12
Cu	7.45	0.73
Fe	31.88	1.39
Mn	34.12	7.37
Ni	15.18	1.46
Si	18.02	2.08
Ti	33.79	2.81
V	37.29	6.20
Zn	2.22	0.56

decrease in electrical conductivity. Thus, more knowledge on the precipitation kinetics of iron-containing constituents upon thermomechanical processing should be gained. In fact, the present study explored the precipitation kinetics of iron in a cold drawn AA1370 aluminium wire. In addition, a new method for metal continuous screw extrusion (MCSE) [16] was applied to produce a wire of identical chemical composition and dimension. The electrical conductivity and mechanical properties were finally compared for wires produced by cold drawing and MCSE.

2. Materials and methods

The commercial aluminium alloy AA1370 has been investigated in this study. It is a common alloy for electric power transmission in wire or rod form. The chemical composition, obtained by mass spectrometry at Norsk Hydro R&D Centre Sunndalsøra, is given in Table 2. Apart from iron and silicon, minor impurities were present. The iron content exceeded the maximum solid solubility given by the equilibrium binary Al-Fe phase diagram [14]. The material was delivered as a Ø3.00 ± 0.02 mm cold drawn wire. The wire had a deformed grain structure, as illustrated by the cross section optical micrograph in Fig. 1.

The cold drawn AA1370 material followed two different investigation paths, see the flowchart in Fig. 2. Firstly, cold drawn wires of AA1370 were prepared for a precipitation study where microstructure, mechanical- and electrical properties were determined. This lead to the development of a novel time–temperature-transformation (TTT)-diagram for precipitation of Fe-rich precipitates in the present aluminium alloy. Secondly, the AA1370 material was granulated and used as feedstock in the novel metal screw extrusion process (MCSE). Electrical and mechanical properties of extruded wires were examined in a similar way as for the cold drawn wire.

Precipitation kinetics of Fe-rich precipitates in the cold drawn wire material was determined by a two-step thermal process. The first step involved solution heat treatment at 640°C for one hour followed by water quenching at 20 °C. This treatment supersaturated the aluminium matrix with iron in solid solution up to 0.052 wt%, i.e. referring to the corresponding phase diagram [14]. A convection oven (Nabertherm HR Chamber) with argon inert gas was used to prevent wire surface oxidation. The solution heat treatment depleted the original deformation structure and induced severe grain growth. Immediately after the solution heat treatment, 'artificial aging' was conducted in a salt bath. Temperatures ranged from 300 to 560 °C and holding times from 10 s to 96 h. All samples were quenched in water after aging.

Further, a Ø3.00 ± 0.20 mm wire of the same composition as the

Table 2
Composition of the investigated alloy AA1370 in wt%.

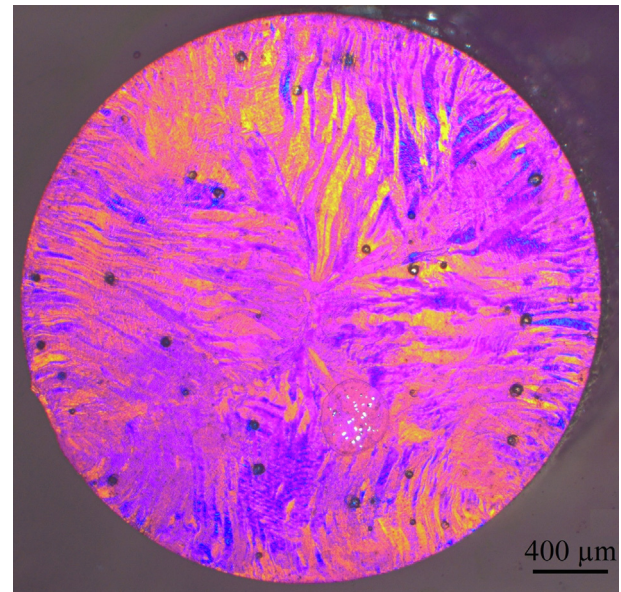| Fe	Si	Zn	Cu	V	Ni	Ti	Mn	Al
0.157	0.058	0.022	0.013	0.006	0.004	0.002	0.001	99.71

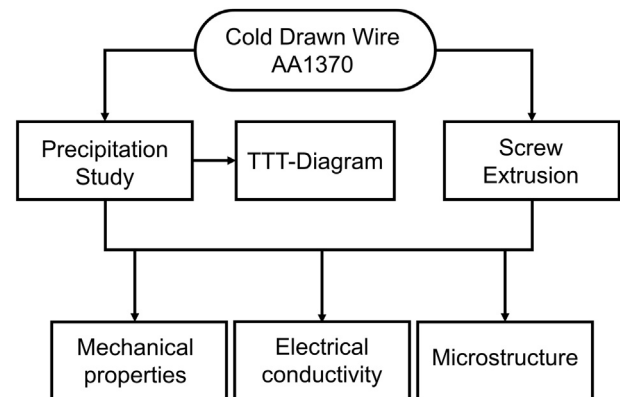**Fig. 1.** Microstructure of AA1370 wire in the cold drawn state (cross section).

Fig. 2. Flowchart for performed activities, showing the two different investigation paths.
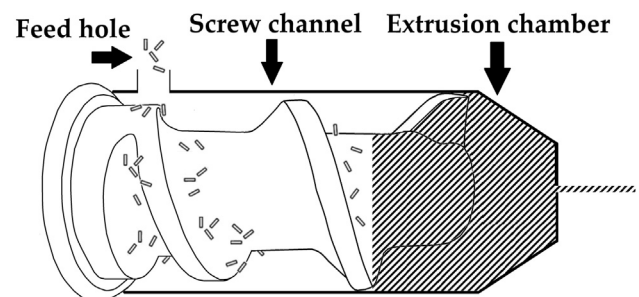

Fig. 3. Conceptual sketch of metallic screw extrusion showing granule material feeding and transport. The feed-stock is consolidated to a solid plug in the hatched area, and extrusion takes place at the right hand end of this area.

cold drawn wire (AA1370, Table 2) was produced by the novel metal screw extrusion process developed by Norwegian University of Science and Engineering (NTNU) and Norsk Hydro [17]. A conceptual sketch of the method is shown in Fig. 3. It comprises of a gear-driven screw covered by a liner to form a screw channel for material transport. By feeding granules of AA1370 at the rear end of the screw through a feed hole, material was transported forward and gradually consolidated. The system was heated externally by a copper induction coil, and internally by screw/metal friction and metal deformation heating. The system

temperatures were monitored by numerous thermocouples located along the screw extruder. Extrusion initiated when the combination of temperature and pressure within the extrusion chamber caused flow through the die opening (i.e. 'break-through'). Detailed descriptions of the process and the inherent material flow processes are outlined elsewhere [16,18]. In other words, cleaned granules of the cold drawn AA1370 material was used as feed-stock for screw extrusion. The process conditions involved a double flight screw and a rotational speed equal 10 rpm, feed-rate 200 g/min and terminal die temperature targeted at 450 $\pm$ 10°C.

Electrical resistance in wires was determined by a microhmmeter (AOIP OM21). The samples had a length of 230 mm, and resistance was measured by sending a pulsed direct current (DC) through the wire length and measuring the corresponding potential drop. Then, the resistance values were converted to electrical conductivity σ, i.e. %IACS (International Annealed Copper Standard) by Eq. 1. Here, L was the distance between the measuring points [mm]; l specimen bar length [mm], R electrical resistance [Ω]; ρ material density [g/mm^3] determined by the chemical composition; and m being the specimens mass [grams]. The constant 58.001 refers to the electrical conductivity in [MS/m] of a pure annealed copper standard having a cross section area equal one square millimeter at 20 °C [19]:

$$\sigma = \frac{Ll}{R\rho m \times 58.001} \times 100\%IACS \qquad (1)$$

Both the drawn wire and the screw extruded material were prepared for microstructural examination through standard metallographic procedures using mechanical grinding with water-lubricated silicon-carbide discs, followed by polishing on cloths with water-based diamond suspensions. Subsequently, a colloidal silica dispersion with particle diameter 0.04 µm was used at the final stage to obtain a mirror-like finish. Grain structures were examined by light optical microscopy applying cross-polarised light and a sub-lambda plate inserted in the column. The polished surface was anodised in Baker's reagent (10 mL HBF$_4$, 400 mL H$_2$O) for 90 s prior to this light optical examination. Scanning electron microscopy (SEM, Zeiss Ultra 55 Ltd.Ed.) in conjunction with electron backscatter diffraction (EBSD) was used to characterise fine-grained areas in the screw extruded cross section wire. Length sections of these wires were examined by transmission electron microscopy (TEM, JEOL JEM-2010). Furthermore, mechanical properties of both types of wire were determined by 1 kilogram force Vickers hardness testing (Matsuzawa DVK-1s) and tensile testing (Zwick/Roell Z2.5). Tensile testing was performed at a strain rate of 3 mm/min, and engineering strain was measured using a LaserXtens optical extensometer. It was considered impractical to machine tensile specimens from the Ø3 mm wires. Copper tubes were instead clamped on the wire ends before tensile testing and served as grips. Here, only samples that fractured far away from the copper grips were considered valid for further analysis.

3. Results

The electrical conductivity-time relation for solution heat-treated and aged samples from cold drawn wire is shown in Fig. 4. Time equal zero represents the supersaturated condition after initial tempering at 640 °C/1 h followed by quenching. All electrical conductivity measurements for the as-quenched condition show a consistent value 62.1 $\pm$ 0.1%IACS. The solution heat-treatment induced a slight increase in electrical conductivity compared to the cold drawn wire, i.e. 61.87%IACS. After prolonged aging at temperatures spanning between 300 and 560 °C, the conductivity eventually increases. The highest achieved conductivity was obtained after aging 400 °C/96 h, i.e. 64.5% IACS. The evolution of iron-rich particles before and after aging is shown in Fig. 5. SEM backscatter electron images processed by the Feature® software show how aging at 400 °C/20 h increased both size and numbers of green Fe-rich phases. The area distribution of detected
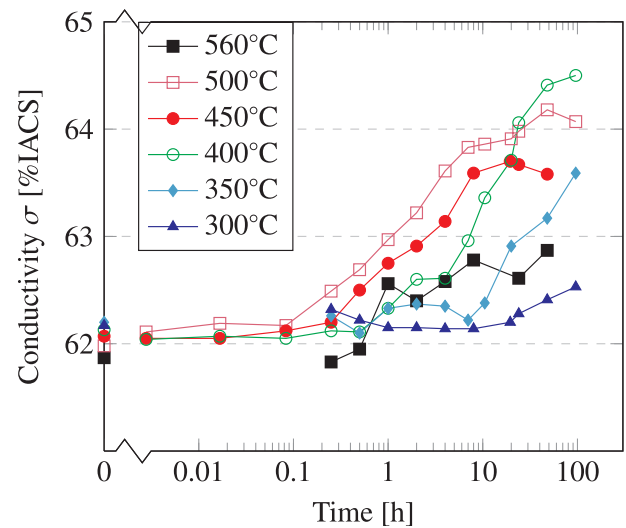

Fig. 4. Electrical conductivity evolution with time at different aging temperatures for cold drawn wire subjected to solution heat treatment at 640 °C/1 h.

particles is shown in Fig. 5c.

By visual inspection of the screw extruded AA1370 wire (Fig. 6b), no visual faults such as blisters or cracks were observed on the wire surface. The extruded wire was completely dense. Metal screw extrusion was therefore proven as an alternative method of producing aluminium conductors as wires and rods. Screw extrusion involves massive plastic deformation on the aluminium material. A newly proposed analytic model by Skorpen [16] evaluated the accumulated strain, ∈, in the current metal screw extrusion set-up. Given the process input parameters, ∈ was in the range of 12–15 for the presented Ø3 mm screw extruded wire.

The screw extruded AA1370 wire showed an electrical conductivity ~64.2%IACS and a tensile strength of 65 MPa. Compared to the commercial benchmark for AA1370 (61.6%IACS, ~85 MPa) [5], the screw extruded wire is softer, but possesses significantly higher conductivity. The original cold drawn wire showed a conductivity of 61.87%IACS, and high ultimate tensile strength, i.e. 164 MPa. It should be noted, however, that the ductility was very low, less than 3% elongation before fracture.

The as-screw extruded wire showed an outer edge consisting of fully recrystallised grains combined with long, tubular grains and subgrains in the centre, Fig. 6. EBSD examinations of as-screw extruded wire revealed presence of a strong ⟨001⟩ cube texture with 64% low angle grain bundaries (LAGB) and an average grain size ~7 µm in the centre region. Corresponding results from TEM examinations of sections containing the extrusion direction are shown in Fig. 7. Here, red arrows indicate positions where grain boundaries were pinned by Fe-rich precipitates, i.e. hampering boundary migration to some extent.

In order to assess the thermal response in the as-screw extruded wire, the material was further aged up to 96 h. The aging temperature was identical to the operation temperature under screw extrusion, i.e. 450°C. The effects of aging on electrical conductivity and hardness are showed in Fig. 8. Artificial aging for 30 min did increase the conductivity slightly, from 64.2%IACS to 64.3%IACS. However, longer aging up to 96 h gradually decreased the electrical conductivity. Besides, internal cracking in the wire material was visible after longer aging time, and the initial centre structure coarsened significantly, see Fig. 9. Despite this microstructure transition, no pronounced effect on hardness was observed, i.e. see Fig. 8.

4. Discussion
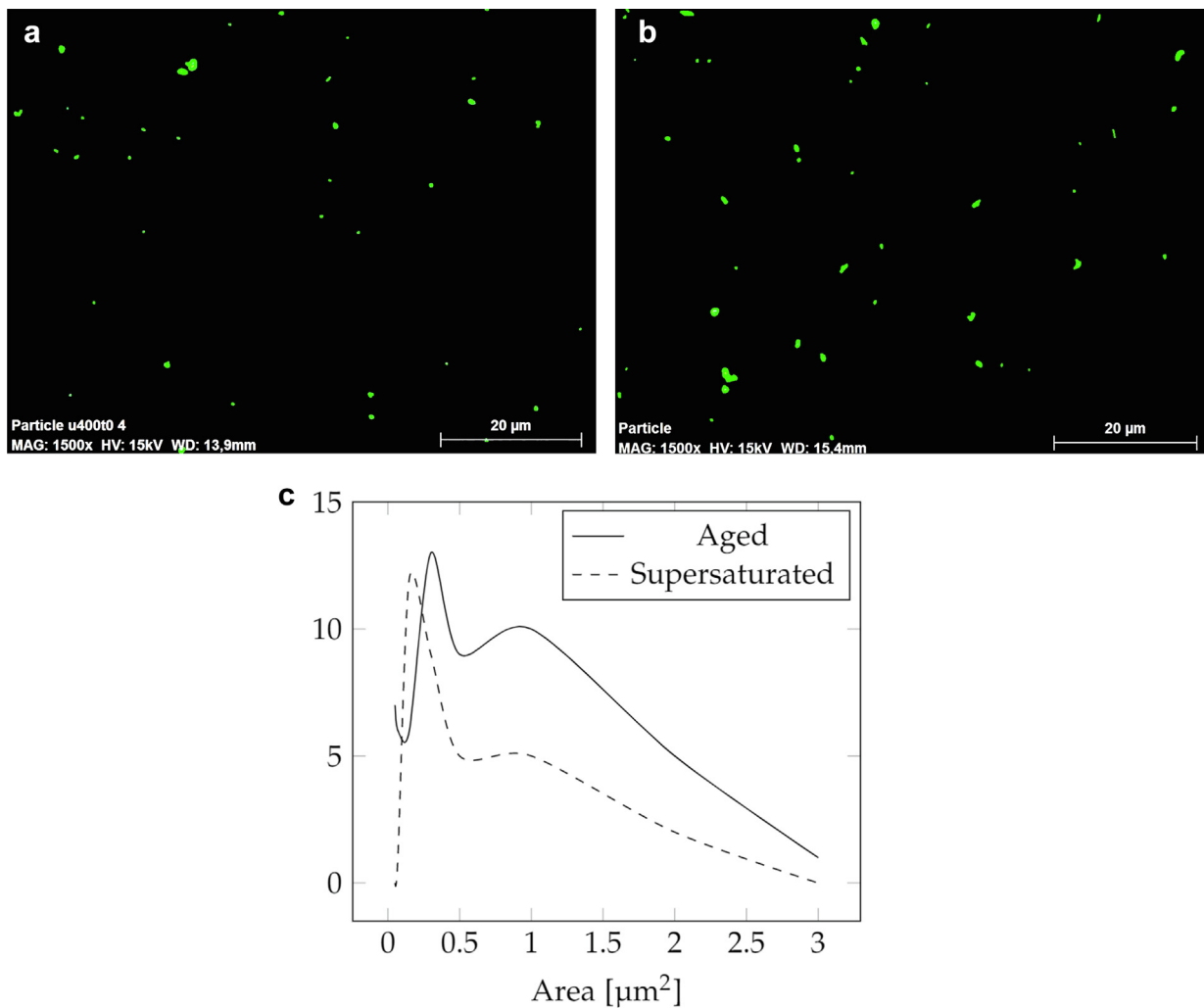
In order to evaluate the relationship between the examined

Fig. 5. SEM backscatter micrographs showing extensive iron-rich particle precipitation after aging of cold drawn wire material.

materials' microstructure, processing method and electrical properties, the contributions which affect the electrical conductivity σ must be estimated. This can be performed through the Matthiessens rule, Eq. 2:

$$\frac{1}{\sigma} = \rho_i + C_v\rho_v + L_d\rho_d + f_{gb}\rho_{gb} + \sum_i C_{sol}^i\rho_{sol}^i \qquad (2)$$

where ρ_i is the intrinsic resistivity of aluminium including the contribution of lattice vibrations, i.e. phonons. Since all electrical conductivity measurements have been performed at 20 °C, ρ_i is regarded as a constant value equal 2.65 $\mu\Omega$cm [13]. The second term in Eq. (2) estimate the effect of vacancies on resistivity. However, all vacancies eventually annihilate at room temperature in commercial pure aluminium [20]. The contribution of vacancies is thus neglected in the following considerations. The effect of dislocations on electrical properties can also be disregarded. Commercial pure AA1XXX alloys can accumulate a maximum dislocation density L_d of 2×10^{14} m^{-2} [21]. Further, theoretical as well as experimental estimations of the constant ρ_d has indicated a value of 2.7×10^{-25} Ω m^3 [22]. The resulting resistivity contribution from dislocations is 5.4×10^{-3} $\mu\Omega$cm, and can be disregarded.

The third term in Eq. 2 take the effect of grain boundaries into account. f_{gb} is the fraction of grain boundaries per unit volume and has a value of $4/D$ for tubular grains, with D being the mean grain size diameter. The specific resistivity from grain boundaries (ρ_{gb}) has been estimated by Karolik and Luhvich [22], i.e. $\rho_{gb} = 2.6 \times 10^{-12}$ Ωcm^2. For tubular grains with diameter equal 1 μm, the resistivity contribution

from grain boundaries can account for 4% of the total resistivity. The effect of grain boundaries can therefore not be neglected.

The resistivity effect of a solute foreign element i (ρ_{sol}^i) can greatly affect the electrical conductivity, as summarised in Table 1. Minor impurity elements such as V, Ni and Ti are assumed to be in solid solution for the AA1370 alloy at all times. Iron and silicon are however present in larger amounts, and can potentially be in solid solution or as AlFe and AlFeSi precipitates [23,24]. The effect of Fe and Si in solid solution (Fe$_{SS}$ and Si$_{SS}$, respectively) is graphically presented in Fig. 10. The electrical conductivity can vary with 2.1%IACS dependent on the state of iron and silicon.

As mentioned in Section 3, the electrical conductivity of the cold drawn wire was 61.87%IACS. After subsequent solution heat treatment at 640°C/1h, the conductivity increased slightly to 62.10%IACS. Since the typical standard deviation for these measurements were ±0.1% IACS, one could claim that the solution heat treatment did only marginally change the electrical conductivity despite a major microstructural transition. It is reasonable to believe that recrystallisation of a fine fibrous structure enhance the electrical conductivity significantly due to the annihilation of grain boundaries. This effect was however largely masked by the supersaturation of iron in solid solution.

Upon subsequent artificial aging of the solution heat treated material, the conductivity gradually increased (Fig. 4). The increase can be related to precipitation of supersatured iron in solid solution into AlFe and/or AlFeSi intermetallics, such as Al$_{13}$Fe$_4$, Al$_5$Fe, Al$_6$Fe, Al$_9$Fe$_2$, Al$_{15}$Fe$_6$Si$_5$ and Al$_9$Fe$_2$Si$_2$ [23]. By considering the time for onset of
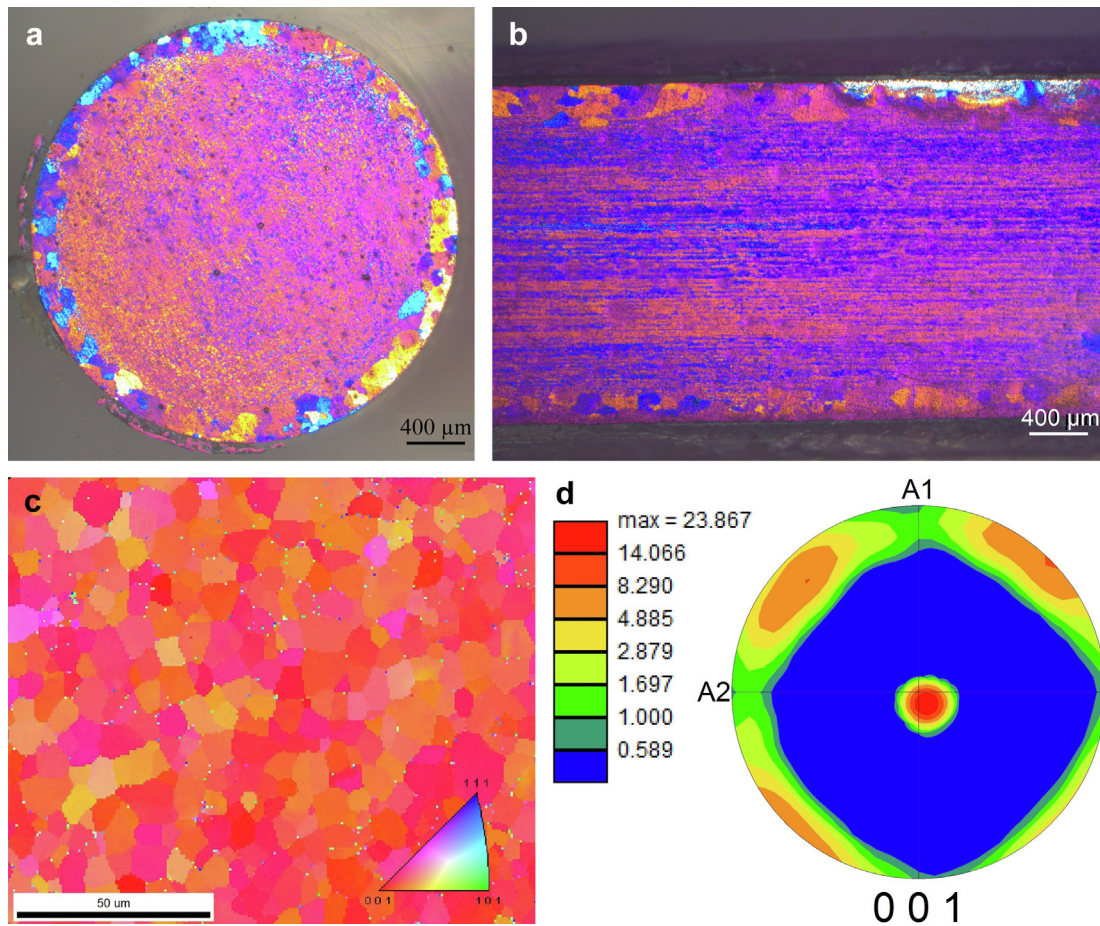
Fig. 6. Microstructure of AA1370 in the as-screw extruded state. A subgrain structure in wire central region is visible.

conductivity increase, the starting point of precipitation can be approximated. A resulting time–temperature-transformation (TTT)-diagram based on such a procedure was in fact developed, thus illustrating the precipitation kinetics of the present AA1370 wire (see Fig. 11). As can be seen, intermediate temperatures in the range of 400–500 °C show the most rapid precipitation kinetics. This can be understood in terms of optimised driving force for precipitation (very low solid solubility of iron), high nucleation rate and reasonable diffusion rate. In fact, the equilibrium solid solubility of iron in aluminium below 450°C is virtually non-existent [14]. Diffusion is however sluggish (iron has a diffusion coefficient less than 1×10^{-12} cm^{2}s^{-1} below 500 °C in pure

aluminium [25]), and shifts precipitation to longer aging times. On the other hand, solute iron diffusion is sufficiently high above 450 °C, but precipitation is restricted by a lower driving force. Belov et al. estimated a threefold increase of iron solubility in aluminium by increasing the temperature from 450 °C to 500 °C [26]. Consequently, precipitation of iron is most rapid at temperatures close to 450 °C.

Moreover, by screw extruding a conductor at 450 °C of equal composition and dimensions as for the drawn wire, a softer yet better conducting material is achievable. In fact, the screw extruded wire reached a conductivity of 64.3%IACS after a short post-aging treatment at 450 °C (Fig. 8). The relative lower strength in the screw extruded
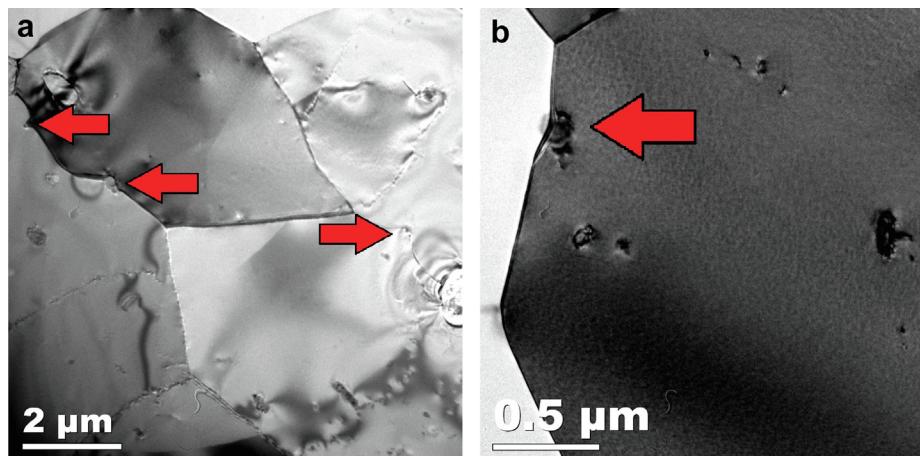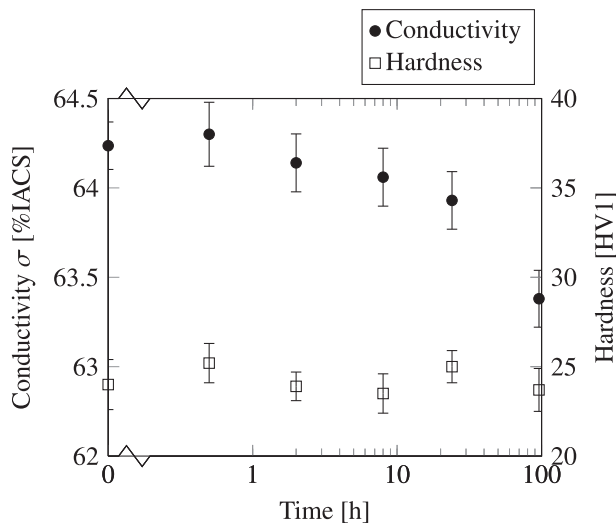

Fig. 7. Bright field TEM images of as-screw extruded wire (extrusion longitudinal view). The red arrows indicate Fe-rich precipitates pinning grain boundaries.
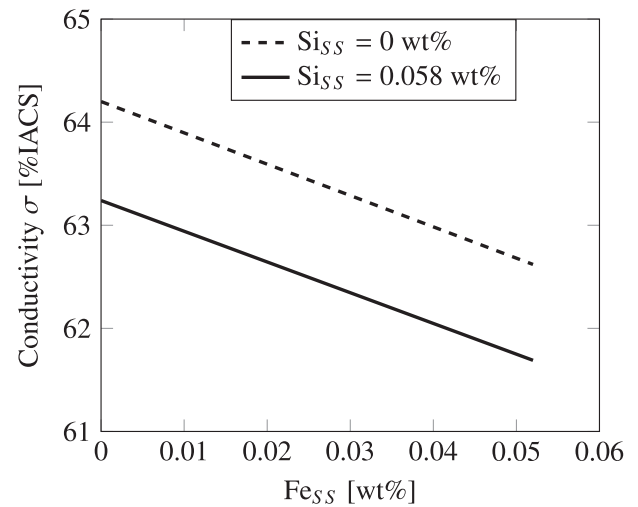
Fig. 8. Electrical conductivity and hardness evolution with time for screw extruded wire during isothermal aging at 450 °C. No solution heat treatment was conducted before aging.

Fig. 10. The effect of the alloying elements iron and silicon in solid solution (Fe_{SS} and Si_{SS}) on electrical conductivity for AA1370. All other impurities are assumed to be in solid solution.

wire can be attributed to dislocation recovery, but do not account for the enhanced electrical conductivity. One possible contribution is due to dynamic recrystallisation and dynamic precipitation of iron-rich precipitates. It is expected that the screw extrusion process exposes the material to a complex thermomechanical history at temperatures in the range between 400 and 450 °C, which is not yet fully understood. As indicated by the TTT-diagram in Fig. 11, aging at 450 °C yield favourable kinetics for iron precipitation. The TEM investigations indicate excessive formation of iron-rich precipitates at grain boundaries, hence increasing the electrical conductivity. Iron particles also act as grain refiners by Zener pinning, i.e. restricting recrystallisation and grain growth (see Fig. 6b). Consequently, the Fe-rich precipitates also preserve the ⟨0 0 1⟩ cube texture.

Another possible contribution to the enhanced electrical properties of the screw extruded wire is the role of a inherent cube texture as shown in Fig. 6d. Long elongated grains which align with the wire length direction (Fig. 6c) coincide with the preferred electron travel direction. According to Mondolfo [27], the cube texture and elongated grains can enhance electrical conductivity up to 1%IACS. However, the related Taylor factor of the cube texture is low, hence macroscopic deformation requires smaller stresses to proceed deformation by slip [28].

Aluminium conductors are utilised for high-voltage applications operating with alternating current (AC). Therefore Eddy currents may

occur from the AC force, and conducting electrons are transported in the outer wire periphery by the so-called skin effect [29]. The screw extruded wire in Fig. 6a has a recrystallised grain structure at its periphery. This structure mainly arose by increased deformation and heat from friction between extruded metal and the extrusion die wall. However, it remains an open question whether this outer recrystallised grain structure with its characteristic texture promotes easy electron transport or not. The cube texture should anyway be promoted in order to obtain excellent electrical conductivity, e.g. by optimising the frictional state and surface flow in the extrusion die. It should also be noted that all results related to electrical conductivity in this study have been performed with DC resistance. The effect of AC mode and skin effect have thus not been explored.

Prolonged tempering of the screw extruded wire induced extensive grain growth in the central part of the wire. The surface grains were however rather unaltered as shown in Fig. 6a and Fig. 9a. Bulk subgrains wire had stored potential energy from the screw extrusion processing, which was released through recrystallisation and grain growth upon subsequent tempering at 450°C. Surface grains was however in a relaxed state, and was not subjected to grain growth. Internal cracking was also observed in the post-tempered wire. The origin of internal cracks in the tempered wire is not known, but is considered to revert both the electrical and mechanical integrity of the material.

For low-load bearing applications such as electrical wiring, mechanical strength can to a large degree be sacrificed for enhanced
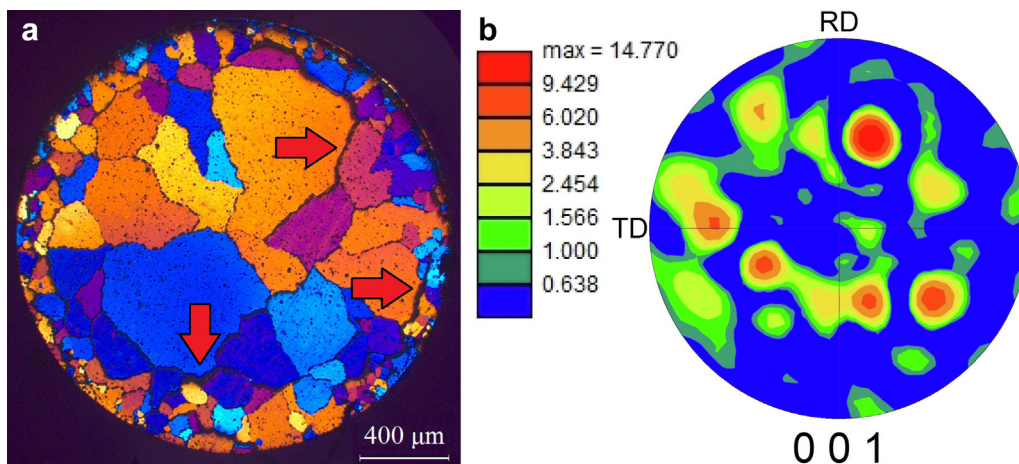
Fig. 9. Microstructure of screw extruded wire in the cross sectional view after aging at 450 °C/96 h. Significant grain coarsening and intergranular cracking (indicated by red arrows) are visible. Please note that the outer layer grain structure did not coarsen to the same extent as for the centre structure (i.e. compare with Fig. 6a). (For interpretation of the references to colour in this figure legend, the reader is referred to the web version of this article.)
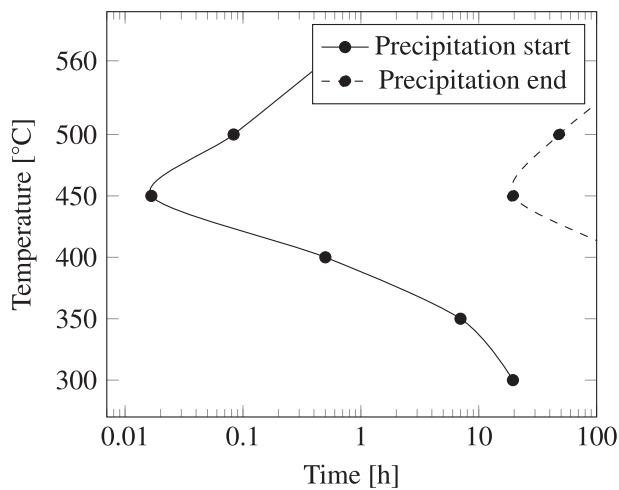
Fig. 11. Established TTT-diagram showing start and end of precipitation for Fe-rich precipitates in cold drawn AA1370 after solution heat treatment and aging to various times at given temperatures.
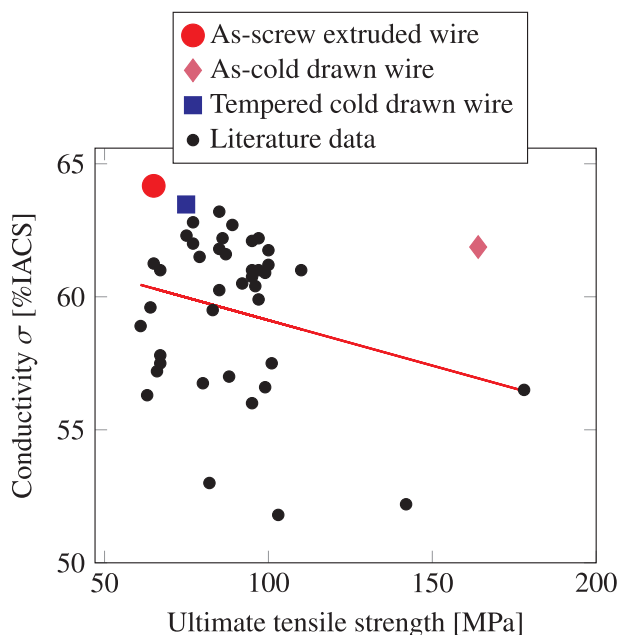

Fig. 12. Tensile strength-electrical conductivity relation for dilute and commercial pure aluminium alloys. The red regression line is based on literature data [5,30–32,24,33,34]. Screw extruded wire processed at 450°C exhibits very high conductivity while being soft (●). As-cold drawn wire is stronger (♦), but with poorer electrical conductivity even after post heat treatment at 450°C/10 min (■).

electrical conductivity. A minimum strength level must however be obtained, in order to avoid premature failing from e.g., creep. In order to further evaluate the combination of properties of the screw extruded wire, a tensile strength-electrical conductivity diagram has been established, Fig. 12. This figure includes reported results from comparable studies for commercial purity aluminium (i.e., AA1XXX alloys) and dilute aluminium alloys in general [30–32,24,33,34]. Most of these alloys exhibit electric conductivity in the range of 52–63%IACS and tensile strengths between 60 and 110 MPa, with some exceptions. An Al-0.5 Mg-0.3Si alloy with and without boron addition shows exceptional strength (142 and 178 MPa, respectively), and reasonable conductivity (52.2 and 56.6%IACS, respectively) [32]. Grain refinement and particle strengthening were proposed for explaining the good combination of properties. Another well-performing conductor is the

AA1370 cold drawn wire used in this study, having high strength and medium conductivity. Tempering of this cold drawn wire at 450 °C/10 min implies a significant decrease in tensile strength combined with a slight increase in electrical conductivity. However, the best electrical conductor of all included alloys in Fig. 12 is the screw extruded wire, with conductivity 64.2%IACS in the as-processed state. The strength is, however, at the lower bound with 65 MPa. Hence, screw extruded wires could favourably be utilised for low load-bearing applications. The strength could in fact be raised by performing screw extrusion at lower temperature, by post-processing such as a slight drawing operation or addition of incoherent ceramic nanoparticles. Nevertheless, the screw extruded product outperform several comparable materials in terms of the strength-conductivity combination.

5. Conclusions

Iron-rich precipitates play a significant role for the cold drawn AA1370 aluminium electrical conductor. Electrical conductivity is greatly enhanced by promoting precipitation of iron. An established TTT-diagram shows Fe-rich particle precipitation kinetics being most rapid at 450 °C.

The investigated AA1370 aluminium alloy has also been processed by novel metal screw extrusion at 450 °C. The as-screw extruded wire outperforms similar alloys in terms of the tensile strength-electrical conductivity combination. Iron-rich particles precipitate at grain boundaries, which pin boundary movements and prevent re-crystallisation and grain growth at elevated temperatures. A pronounced ⟨0 0 1⟩ fiber texture seems to enhance the electrical conductivity. However, the optimum microstructure in the surface area of conducting wires remains an open question.

Data availability

The raw data required to reproduce these findings cannot be shared at this time due to technical or time limitations. The processed data required to reproduce these findings cannot be shared at this time due to technical or time limitations.

Declaration of Competing Interest

The authors declare that they have no known competing financial interests or personal relationships that could have appeared to influence the work reported in this paper.

References

[1] F. Kiessling, P. Nefzger, J.F. Nolasco, U. Kaintzyk, Overhead Power Lines: Planning, Design, construction, 1st ed., Springer, 978-3-642-05556-0, 2003.

[2] S. Karabay, Modification of AA-6201 alloy for manufacturing of high conductivity and extra high conductivity wires with property of high tensile stress after artificial aging heat treatment for all-aluminium alloy conductors, Mater. Design 27 (2006) 821–832, https://doi.org/10.1016/j.matdes.2005.06.005.

[3] R.H. Kemsies, B. Milkereit, O. Kessler, T. Fuhrmann, S. Schlegel, F. Plonus, S.P. Miller-Jupp, J. Hirsch, Effect of dispersoids on long-term stable electrical aluminium connections, Materials Science Forum 877 (2017) 409–415, https://doi.org/10.4028/www.scientific.net/MSF.877.409.

[4] G.E. Marcantoni, From molten metal to 3.2 mm wire for mechanical applications, Light Metals (2012 (2012)) 251–255, https://doi.org/10.1007/978-3-319-48179-1_44.

[5] SAE, ASTM, Metals and Alloys in the Unified Numbering System, SAE Publications, 8th edition, 1999. ISBN 0-7680-0407-1.

[6] P. Drude, Zur elektronentheorie der metalle, Annalen der, Physik 306 (1900) 566–613, https://doi.org/10.1002/andp.19003060312.

[7] A. Matthiessen, M. von Bose I., On the influence of temperature on the electric conducting power of metals, Philos. Trans. R. Soc. London 152 (1862) 1–27, https://doi.org/10.1098/rstl.1862.0001.

[8] J. Miyake, M. Fine, Electrical conductivity versus strength in a precipitation hardened alloy, Acta Metallurgica et Materialia 40 (1992) 733–741, https://doi.org/10.1016/0956-7151(92)90015-7.

[9] M. Mujahid, N. Engel, E. Chia, Effect of alloying elements on the conductivity of aluminum alloys, Scr. Metall. 13 (1979) 887–893, https://doi.org/10.1016/0036-9748(79)90181-9.

[10] F. Kutner, G. Lang, Effect of addition elements and heat-treatment on the specific electrical resistivity, Aluminium 52 (1976) 322–326.

[11] S. Bera, I. Manna, Synthesis of CuCr and CuCrAg alloy with nano-ceramic dispersion by mechanical alloying and consolidation by laser assisted sintering, Mater. Chem. Phys. 132 (2012) 109–118, https://doi.org/10.1016/j.matchemphys.2011.11.005.

[12] S. Bera, S.G. Chowdhury, W. Lojkowsky, I. Manna, Synthesis of CuCr and CuCrAg alloys with extended solid solubility with nano-Al2O3 dispersion by mechanical alloying and consolidation by high pressure sintering, Mater. Sci. Eng.: A 558 (2012) 298–308, https://doi.org/10.1016/j.msea.2012.08.004.

[13] J.E. Hatch, Aluminium: Properties and Physical Metallurgy, American Society for Metals, 1st edition, 1984. ISBN 0-87170-176-6.

[14] X. Li, A. Scherf, M. Heilmaier, F. Stein, The Al-rich part of the Fe-Al phase diagram, J. Phase Equilibria Diffusion 37 (2016) 162–173, https://doi.org/10.1007/s11669-015-0446-7.

[15] K. Ito, R. Musick, K. Lücke, The influence of iron content and annealing temperature on the recrystallization textures of high-purity aluminium-iron alloys, Acta Metallurgica 31 (1983) 2137–2149, https://doi.org/10.1016/0001-6160(83)90033-0.

[16] K.G. Skorpen, 2018:218 Screw Extrusion of Light Metals, Ph.D. thesis, Norwegian University of Science and Technology, 2018. URL: http://hdl.handle.net/11250/2565656.

[17] J.C. Werenskiold, L. Auran, H.J. Roven, N. Ryum, O. Reiso, Screw extruder for continuous extrusion of materials with high viscosity, 2008. WO 2008/063076, EP 2086 697 B1.

[18] F. Widerøe, T. Welo, Using contrast material techniques to determine metal flow in screw extrusion of aluminium, J. Mater. Process. Technol. 213 (2013) 1007–1018, https://doi.org/10.1016/j.jmatprotec.2012.11.013.

[19] S.W. Stratton, Copper Wire Tables, Technical Report 31, Circular of the Bureau of Standards, 1914. URL: http://www.archive.org/stream/copperwireTable 31unituoft#page/n5/mode/1up.

[20] F.R. Fickett, Aluminum-1. A review of resistive mechanisms in aluminum, Cryogenics 11 (1971) 349–367, https://doi.org/10.1016/0011-2275(71)90036-1.

[21] H. Adachi, Y. Miyajima, M. Sato, N. Tsuji, Evaluation of dislocation density for 1100 aluminum with different grain size during tensile deformation by using in-situ X-ray diffraction technique, Mater. Trans. (2015), https://doi.org/10.2320/matertrans.L-M2015803 L-M2015803.

[22] A.S. Karolik, A.A. Luhvich, Calculation of electrical resistivity produced by dislocations and grain boundaries in metals, J. Phys.: Condensed Matter 6 (1994) 873, https://doi.org/10.1088/0953-8984/6/4/007.

[23] P. Skjerpe, Intermetallic phases formed during DC-casting of an Al- 0.25 wt pct Fe-0.13 wt pct Si alloy, Metall. Mater. Trans. A 18 (1987) 189–200, https://doi.org/10.1007/BF02825700.

[24] Q. Zhao, Z. Qian, X. Cui, Y. Wu, X. Liu, Optimizing microstructures of dilute Al–Fe–Si alloys designed with enhanced electrical conductivity and tensile strength, J. Alloys Compd. 650 (2015) 768–776, https://doi.org/10.1016/j.jallcom.2015.08.052.

[25] G. Hood, The diffusion of iron in aluminium, Philos. Mag. 21 (1970) 305–328, https://doi.org/10.1080/14786437008238419.

[26] N.A. Belov, A.A. Aksenov, D.G. Eskin, Iron in Aluminium Alloys: Impurity and Alloying Element, 1st ed., Taylor & Francis, 2002 ISBN 0-415-27352-8.

[27] L.F. Mondolfo, Aluminum Alloys: Structure and Properties, 1st ed., Elsevier, 2013 ISBN 0-408-70932-4.

[28] Q. Liu, X. Huang, D. Lloyd, N. Hansen, Microstructure and strength of commercial purity aluminium (AA 1200) cold-rolled to large strains, Acta Materialia 50 (2002) 3789–3802, https://doi.org/10.1016/S1359-6454(02)00174-X.

[29] H.A. Wheeler, Formulas for the skin effect, Proc. IRE 30 (1942) 412–424, https://doi.org/10.1109/JRPROC.1942.232015.

[30] F. Pan, D. Edmonds, S. Zhou, P. Ding, Effects of rare earth metals on electrical conductivity and mechanical properties of commercial purity aluminium, Mater. Sci. Technol. 10 (1994) 933–935, https://doi.org/10.1179/mst.1994.10.11.933.

[31] Q. Zhao, X. Cui, Z. Qian, X. Liu, The synergistic effect of Al–B–C master alloy to improve conductivity and strength of 1070 alloy, J. Alloys Compd. 639 (2015) 478–482, https://doi.org/10.1016/j.jallcom.2015.03.091.

[32] X. Cui, Y. Wu, G. Zhang, Y. Liu, X. Liu, Study on the improvement of electrical conductivity and mechanical properties of low alloying electrical aluminum alloys, Compos. Part B: Eng. 110 (2017) 381–387, https://doi.org/10.1016/j.compositesb.2016.11.042.

[33] X. Cui, Y. Wu, X. Liu, Q. Zhao, G. Zhang, Effects of grain refinement and boron treatment on electrical conductivity and mechanical properties of AA1070 aluminum, Mater. Des. 86 (2015) 397–403, https://doi.org/10.1016/j.matdes.2015.06.149.

[34] H.C. Liao, Y. Liu, C. Lü, Q.G. Wang, Effect of Ce addition on castability, mechanical properties and electric conductivity of Al–0.3 Si–0.2 Mg alloy, Int. J. Cast Metals Res. 28 (2015) 213–220, https://doi.org/10.1179/1743133615Y.0000000002.